Microstructure and tribological properties of WS_x/a-C multilayer films with various layer thickness ratios in different environments

Fang-er Yang, Ye Lu, Rong Zhang, Xiang-hua Zhang, Xiao-hua Zheng

PII: S0257-8972(16)31203-8
DOI: doi: 10.1016/j.surfcoat.2016.11.071
Reference: SCT 21817

To appear in: *Surface & Coatings Technology*

Received date: 3 July 2016
Revised date: 18 October 2016
Accepted date: 19 November 2016

Please cite this article as: Fang-er Yang, Ye Lu, Rong Zhang, Xiang-hua Zhang, Xiao-hua Zheng, Microstructure and tribological properties of WS_x/a-C multilayer films with various layer thickness ratios in different environments, *Surface & Coatings Technology* (2016), doi: 10.1016/j.surfcoat.2016.11.071

Microstructure and tribological properties of WS_x/a-C multilayer films with various layer thickness ratios in different environments

Fang-er Yang[a], Ye Lu[a], Rong Zhang[a], Xiang-hua Zhang[b], Xiao-hua Zheng[a*]

[a] *College of materials science and engineering, Zhejiang University of Technology, Hangzhou 310014, China*

[b] *Laboratoire des Verres et Céramiques, UMR CNRS N° 6226 ISCR, Université de Rennes 1, Campus de Beaulieu, Rennes Cedex 35042, France*

Abstract: WS_x/a-C multilayer films with different layer thickness ratios and the modulation period of ~50 nm were prepared on monocrystalline silicon substrate by magnetron sputtering method. The morphology, microstructure and composition of the films were characterized by using scanning electron microscopy (SEM), X-ray diffractometry (XRD), energy dispersive X-ray spectroscopy (EDS) and Raman spectroscopy. The surface chemical states under different etching conditions were investigated by X-ray photoelectron spectroscopy (XPS) depth profile technique. The hardness, the adhesion to the substrate and the tribological properties of the films under various test environments were evaluated by means of nano-indentation, scratching tester and ball-on-disk tribometer. The results showed that a WS_2 phase with (101) preferential orientation was formed in WS_x sublayer and the WC phase was not present at the WS_x/a-C interface. The effects of $L_{a\text{-}C}/L_{WSx}$ ratio on the microstructure of as-prepared films were negligible while the effects on the

* Corresponding author. Tel. +86 571 88320479. Fax: +86 571 88320479

E-mail: zhengxh@zjut.edu.cn (X. H. Zheng)

mechanical and tribological properties of the film were significant. An increased hardness (the maximum of ~2.2 GPa) and a decreased adhesion were found in the multilayer films. The WS_x/a-C multilayer films were of the best wear resistance in vacuum (the minimum of 5.7×10^{-15} m^3 $N^{-1}m^{-1}$) and exhibited much better tribological properties than a single WS_x film in various test environments.

Keywords: WS_2; a-C; multilayer film; friction and wear; magnetron sputtering

1. Introduction

As a solid lubricant, WS_2 has been widely used in low temperature and aerospace environments due to its excellent performance of high bearing capacity, low friction coefficient, high wear resistance and so on [1, 2]. However, the friction coefficient increases and the wear resistance deteriorates greatly when it serves in humid air. The main reason is that the dangling bonds on the edge of WS_2 crystals are more chemically active and can easily be oxidized in oxygen or humid atmosphere [3-5], which limits the scope of its application.

Recent studies showed that the addition of metallic elements to WS_2 film such as Cr [6], Ag [7, 8], Cu [9], Ti [10] could densify the film, thereby increase the hardness and the adhesion to substrate and improve the wear resistance of the film. The doping of nonmetallic elements such as C and/or N [11-15] could destroy the columnar morphology, greatly increase the hardness and adhesion of the film due to the presence of W-C and/or W-N phase and lead to a significantly improved wear resistance. Moreover, the WC/DLC/WS_2 nanocomposite film [16, 17] also showed a

better tribological performance than WS_2 film.

Since the nanometer-scale multilayer film was expected to exhibit good mechanical properties, the WS_2/MoS_2 multilayer films [18-20] were also investigated. The relevant results showed that the WS_2/MoS_2 multilayer films were of low friction coefficients and long endurance life in comparison to those of the individual single-layer materials in atmosphere and/or in vacuum. Based on the results above and the excellent tribological properties of amorphous carbon (a-C) in humid air [21], the addition of a-C layer to WS_x film is expected to fabricate a WS_x/a-C multilayer film with better tribological performance in humid air. In this paper, the WS_x/a-C multilayer films with various layer thicknesses ratios of a-C to WS_x (*i.e.* $L_{a\text{-}C}/L_{WSx}$, or modulation ratio) have been prepared by RF magnetron sputtering technique. The microstructure and tribological properties of the films in vacuum, in humid air and in distilled water have been investigated. Also, the effects of $L_{a\text{-}C}/L_{WSx}$ on microstructure, mechanical and tribological properties of the films and the role of the a-C sublayer have been discussed.

2. Experimental

2.1 *Film preparation*

WS_x/a-C multilayer films were deposited on Si (111) wafer substrates by sputtering alternately WS_2 target (99.9 wt.% in purity, 60 mm in diameter) and graphite target (99.99 wt.% in purity, 60 mm in diameter) in Ar gas atmosphere. The silicon substrate was degreased ultrasonically in acetone and absolute alcohol for 15

min in each solvent, then etched in an aqueous solution of HF (10 vol.%) for 20 min and rinsed with distilled water. After being dried with nitrogen gas, the substrate was loaded rapidly into the vacuum chamber (JGP-450 fast ion plating apparatus) in which the spinning substrate can be switched to the position in front of each target. Before deposition, the chamber was evacuated to 1×10^{-3} Pa. The depositions were performed at room temperature. The pressure of Ar gas (99.999 wt.% in purity) was fixed at 1.0 Pa and the sputtering power was set at 80 W for graphite target and 90 W for WS_2 target. A pulsed DC bias voltage of -50 V (duty factor 50%) was applied to the substrate during the deposition. The multilayer film samples were deposited by controlling the exposure time of the substrate to the graphite target or WS_2 target. The computer-operated target baffle in front of the target was used to control the exposure time. The baffle was quickly opened at the beginning of the deposition and closed at the end of the deposition duration of the target, and then the substrate was switched to the position in front of the other target. The plasma was always turned on during the deposition and the WS_x sublayer was deposited firstly. The modulation period was about 50 nm. The layer thickness ratios $L_{a\text{-}C}/L_{WSx}$ of 1:39, 1:19, 1:9, 3:20 and 1:4 inside each period have been studied. The layer thickness ratio was calculated according to the measured thickness of WS_x sublayer and the deposition rate of a-C sublayer (due to a constant rate of 2.085±0.037 nm/min). The total number of modulation periods was 20 and consequently the total thickness of the films was around 1 μm. For comparison, a single WS_x film (3.3 μm in thickness) and single a-C film (0.45 μm in thickness) were prepared under the same process conditions.

2.2 *Characterization of the films*

To elucidate the phase structure of the films, the X-ray diffraction experiments were carried out by using a X-ray diffractometer (X'PERT PRO, X'Celerator detector, Cu Kα radiation, tube voltage of 40 kV, tube current of 40 mA, scanning velocity of 0.033 °/s). The surface and the cross-section morphology of the films were observed by using a field emission scanning electron microscope (Zeiss, ∑IGMA) with an accelerating voltage of 15 kV. The chemical compositions of the films were analyzed by the energy dispersive X-ray spectrometer (EDS) attached to the microscope. The X-ray photoelectron spectra of the films were collected by using an X-ray photoelectron spectrometer (Kratos Axis Ultra DLD, monochromatic Al Kα excitation source, power of 45 W, resolution of 0.68 eV, energy step of 0.05 eV, pass energy of 20 eV). The samples were etched by Ar^+ ion with kinetic energy of 4.8 keV for various durations. The standard etching rate, calibrated with Ta_2O_5 is 1nm/min. The energy calibration was performed with Cu $2p_{3/2}$ line (932.67 eV) and Ag $3d_{5/2}$ line (368.26 eV). The spectrum fitting was performed by using XPSPEAK software, Shirley method was used to deduct the background and Gaussian-Lorentzian function was used to fit the curve. The vibration mode of a-C film was analyzed by using a laser micro Raman spectrometer (LabRAM HR UV, Yvon Jobin, laser wavelength of 632.8 nm, detection range of 400~3000cm^{-1}). Linear interpolation method was used to deduct the background and the spectrum was fitted with Gaussian-Lorentzian function in LABSPEC software.

The hardness of the films was measured by using a nano-indenter (Nano Indenter G200, Agilent) with a maximum load of 0.6 mN and the continuous stiffness method. The adhesion of the films was evaluated by using a scratch tester (WS-2005) with scratching speed of 4 mm/min, scratching distance of 4 mm, loading rate of 100 N/min, and the maximum load of 100 N. The tribological behavior of the films in vacuum (10^{-2} Pa), in humid air (relative humidity ≈70%) and in distilled water was evaluated by using a ball-on-disc tribotester (WTM-1E). The films served as the disk and the Si_3N_4 ceramic balls (1200HV in hardness and 3 mm in diameter) acted as the coupled part. The tests were performed at a normal load of 0.49 N and a sliding speed of 0.105 m/s for 15 minutes. The average values of the instantaneous friction coefficient in the specific range of sliding time were used and the wear rates were calculated from the abrasion volume measured by using a profilometry (Dektak3).

3. Results and discussion

3.1 *Composition and microstructure*

Fig.1 shows the SEM morphologies of the films. It can be seen from Fig.1a that the surface of the single WS_x film is composed of small stick-like crystals, while the single a-C film is composed of small closely packed blocks (30~50 nm in size). The morphology of the multilayer films exhibits a combination of stick-like crystals and small blocks. The size of the blocks is significantly larger than that of the single a-C film and the effect of $L_{a\text{-}C}/L_{WSx}$ ratio is very weak. As shown in Fig.1b, the back scattered electron (BSE) images of the multilayer films both exhibit the layered

structure, in which the bright strip corresponds to WS_x layer and the gray strip corresponds to a-C layer. The interface between WS_x layer and a-C layer near the substrate is very straight. According to the total thickness of the multilayer films and the total number of modulation periods, the average period of the multilayer films are about 51.7 nm for $L_{a\text{-}C}/L_{WSx}$=1:19 and 53.2 nm for $L_{a\text{-}C}/L_{WSx}$=1:4 respectively, which close to the designed values.

The EDS results are listed in Table 1. There exist S, C, W and O elements in the films. It can be seen that the S/W ratio of the films is between 1.38 and 1.62, indicating a certain loss of S element during the deposition process, which is in agreement with the results reported in the literatures [22, 23]. With the increase of $L_{a\text{-}C}/L_{WSx}$ ratio, the S/W ratio of the multilayer films also increases and it is higher than the ratio for the single WS_x film. It means that the addition of a-C layer can significantly raise the sulphur content in WS_x layer. The possible reason is that the coverage of a-C layer onto WS_x layer can prevent the WS_x layer from being bombarded by high energy species and then restrain the loss of sulphur element from the WS_x layer. The thinner the WS_x layer thickness is, the shorter the bombarded duration of the WS_x layer is. Consequently, the sulphur content of WS_x layer increases with increasing the $L_{a\text{-}C}/L_{WSx}$ ratio.

The XRD patterns of the films are shown in Fig.2. The diffraction peak of WS_2 (101) appears in the single WS_x film and the peak (002) is very weak, indicating that the single WS_x film is of (101) preferential orientation and somewhat different from the type I WS_2 named by P D Fleischauer [24, 25]. The single a-C film has a

microcrystalline or amorphous structure without the presence of the peaks neither from graphite nor from diamond. The peak at 2theta of ~28.4° in all patterns is attributed to the Si substrate. Compared to the single WS_x film, the multilayer films show a significantly weaker peak intensity of WS_2 (101). This is easily understandable as the content of WS_2 phase in the films decreases with increasing the $L_{a\text{-}C}/L_{WSx}$ ratio. Since the atomic percentage of WS_x layer (*i.e.* the sum of the content of W and S, Table 1) is 62.8% in the sample with $L_{a\text{-}C}/L_{WSx}$ ratio of 1:19 and only 53.0% in the sample with $L_{a\text{-}C}/L_{WSx}$ ratio of 1:4, significantly lower than that of the single WS_x film, it is considered that the decreased content of WS_x layer in the multilayer films leads to the decreased diffraction intensity of WS_2 phase in both samples. In addition, the diffraction peaks of WC phase are not observed in the multilayer films, confirming the absence or the very low concentration of crystalline WC phase.

Fig.3 shows the Raman spectrum of the a-C layer of the sample with $L_{a\text{-}C}/L_{WSx}$ ratio of 1:19. The recent studies show that the Raman spectrum of the a-C films is composed of D peak (~1350 cm^{-1}) and G peak (~1560 cm^{-1}). The D peak is derived from the disordered structure [26-29] and the area ratio of D peak to G peak (I_D/I_G) corresponds to the content of sp^3 bonds in a-C film [30, 31]. In Fig.3, the deconvolution results show that the spectrum of the a-C layer is composed of D peak (centered at 1350 cm^{-1}) and G peak (centered at 1523 cm^{-1}) with an I_D/I_G ratio of 0.25, corresponding to the typical characteristic of magnetron sputtered a-C films [28, 31, 32].

Fig.4 shows the XPS spectra of O_{1s}, S_{2p}, C_{1s}, W_{4f} and their fitting results of the sample with $L_{a\text{-}C}/L_{WS_x}$ ratio of 1:19 under different etching durations. In Fig.4a, the O_{1s} spectrum before etching (*i.e.*, etching duration 0 s) can be deconvoluted into three peaks [33-35] centered at binding energy (B.E.) of 530.8 ±0.1 eV (illustrated in vertically dashed line), 531.9 ±0.1 eV and 533.1 ±0.1 eV, corresponding to the W-O (WO_3), C-O and H-O bonds respectively. With the increase of the etching duration from 0 s to 360 s, the three peaks almost lie at the same position and the latter two peaks become weaker and their area percentage considerably drops, indicating that the percentage of both C-O and H-O bonds decreases. Further increase in etching duration (960 s) leads to a still weaker C-O peak and the disappearance of the H-O peak. This is expected since the C-O and H-O bonds can mainly be attributed to the exposure of the sample in humid air and can be eliminated during the etching. However, the permanent presence of W-O peak throughout the etching process indicates a low oxidation resistance of WS_x during the exposure of the film in the atmosphere. In Fig.4b, the S_{2p} spectrum can be decomposed into four peaks centered at 162.0 ±0.1 eV (illustrated in vertically dashed line), 163.2 ±0.1 eV, 163.5 ±0.1 eV and 164.7 ±0.1 eV during the etching process, corresponding to the $2p_{3/2}$ and $2p_{1/2}$ line of S element from WS_2 and WO_xS_y respectively [36, 37]. With increasing etching duration from 0 s to 960 s, the total area percentage of the latter two peaks drops from 64.6% to 16.9%, indicating that the WO_xS_y is partially removed as a surface contaminant by the etching. In Fig.4c, the C_{1s} spectrum before etching can be deconvoluted into four peaks [38, 39] centered at the binding energy of 284.5 ±0.1 eV

(illustrated in vertically dashed line), 285.3 ±0.1 eV, 286.2 ±0.1 eV, and 288.3 ±0.2 eV, corresponding to the sp^2C-C, sp^3C-C, C-O and C=O bonds respectively. Since the contents of sp^2C-C and sp^3 C-C bonds can be calculated by using the area ratio of these peaks [40], the ratio of sp^3C-C to sp^2C-C in the a-C layer is then evaluated and a value of 0.22 is found. These results indicate that the sp^2C-C bond is largely dominating in the C layer. However, the C1s spectrum under both etching duration of 60 s and 360 s can be fitted by the first two peaks only, since the oxygen content drops due to the etching and the C content decreases from 72.4 at.% before etching to 55.7 at.% after an etching during 360 s. After an etching during 960 s, the C1s spectrum can only be fitted by one peak centered at 284.4 ±0.1eV and the C content at this moment is about 33.5 at.%. Considering the absence of the W-C bond (binding energy locating at 282.9 eV), we can conclude that the WC phase is not formed in the present film. Concerning the sample after an etching during 960 s, its spectra should be derived from the WS_x layer with therefore a very low C content (less than 1 at.%). The possible reason for the high C content in this case could be that the interface between the top a-C layer and the top WS_x layer is not an ideal plane or/and the long-time ion etching leads to the appearance of carbon contaminant on the surface. In Fig.4d, the W_{4f} spectrum before etching can be deconvoluted into four peaks [41, 42], in which the binding energies centered at 32.6 ±0.1 eV (illustrated in vertically dashed line) and 34.8 ±0.1 eV are attributed to WS_2, and 35.8 ±0.1 eV and 38.0 ±0.1 eV (illustrated in vertically dashed line) to WO_3. WO_3 phase is the major component on the surface of the film because of the oxidation during the exposure of the film in the

atmosphere. As for the W_{4f} spectra after different etching durations, all of them can be decomposed into six peaks. The peaks located at ~32.7 eV and ~34.9 eV are assigned to WS_2 and those centered at ~35.7 eV and ~37.9 eV are assigned to WO_3, very close to the spectrum before etching. However, at the low binding energy side, the additional peak doublet is attributed to non-stoichiometric oxide WO_x (x<2) [43] and its position shifts to a lower energy as increasing the etching duration from 60 s to 960 s. Since the positive correlation between S/W ratio and the peak position of WO_x is observed in our experiments with respect to the etching of single WS_x film, we confirm that the shift of peak position of WO_x in the sample with $L_{a\text{-}C}/L_{WSx}$ ratio of 1:19 is attributed to the decrease of S/W ratio (from 1.15 to 0.49). The decrease of S/W ratio is easily understandable since WS_2 is prone to decompose at high temperature induced by the etching with high ion energy of 4.8 keV, leading to a significant loss of element S.

Based on the similarity of XPS spectra between the sample with $L_{a\text{-}C}/L_{WSx}$ ratio of 1:19 and the single WS_x film, it can be concluded that there is no obvious change in phase structure of the a-C layer and WS_x layer in multilayer films. The main reason is that the deposition of the film is conducted at room temperature.

3.2 *Hardness and adhesive strength of the films*

Fig.5 shows the dependence of the hardness and the adhesive strength of the films with different $L_{a\text{-}C}/L_{WSx}$ ratios. In Fig.5a, the hardness of the multilayer films reaches the maximum at the $L_{a\text{-}C}/L_{WSx}$ ratio of 1:9 and is higher than that of the calculated value (black solid bar) based on the rule of mixture. This suggests a positive effect of

interface strengthening in the multilayer films and the inapplicability of the rule of mixture here. As for the single a-C film, since the content of sp^2C-C bond in the film is much higher than that of sp^3C-C bond, its hardness is therefore much lower compared to the DLC films [44]. From Fig.5b, the adhesion of the multilayer films rapidly decreases to reach the lowest value and then increases with an increasing $L_{a\text{-}C}/L_{WSx}$ ratio. We believe that this trend could be attributed to the change of stress distribution induced by the increasing thickness of a-C layer in a modulation period. The detailed stress distribution in the multilayer films needs further study.

3.3 *Tribological properties of the films*

Fig.6 shows the SEM morphologies of the films after tribological tests in different environments. In vacuum, the surface of the single WS_x film (Fig.6a) is characterized by many wear debris, scratches and a large width of wear track, but the film is not removed; on the contrary, the single a-C film (Fig.6j) has been completely worn out and the width of the exposed silicon substrate in the wear track is significantly large than that of the other films. According to Fig.6d and Fig.6g, we can conclude that the wear resistance of the sample with $L_{a\text{-}C}/L_{WSx}$ ratio of 1:19 is obviously better than that of the sample with $L_{a\text{-}C}/L_{WSx}$ ratio of 1:4. The results from SEM observation and EDS element analysis (omitted here) for the wear scar of the Si_3N_4 balls show that adhesive wear is the main wear mechanism between the multilayer films and the Si_3N_4 balls, which is consistent with the literature [45]. In humid air, all of the single WS_x film (Fig.6b), the sample with $L_{a\text{-}C}/L_{WSx}$ ratio of 1:19 (Fig.6e) and the sample with $L_{a\text{-}C}/L_{WSx}$ ratio of 1:4 (Fig.6h) present a larger width of

the wear tracks compared to that of the film in vacuum. This indicates that the wear resistance of the above films in humid air is lower than in vacuum. Based on the observation shown in Fig.6k and Fig.6j, we can conclude that the wear resistance of the single a-C film in humid air is greatly improved in spite of partial peeling on the wear track. The wear mechanism between the multilayer films and the Si_3N_4 balls in humid air is found to be the same as in vacuum. In distilled water, it can be seen that all of the films are worn out (Fig.6c, 6f, 6i, 6l), the exposed silicon substrate exhibits a relatively rough topography with few debris, which may be related to the agitation (or movement) of the distilled water by continuously taking away the wear debris during the tests.

Fig.7 shows the instantaneous friction coefficient of the films as a function of the sliding time. In vacuum (Fig.7a), the instantaneous friction coefficients of the films are more stable after the running-in period (within 25s) except the single a-C film. An abrupt increase then apparent fluctuation of the instantaneous friction coefficient of the single a-C film after a sliding time of 230s suggests an obvious change of the contact state between the film and the ceramic ball. The ball will directly slide on the surface of Si substrate when the film is worn out (see Fig.6j). In humid air (Fig.7b), a more stable instantaneous friction coefficient is presented for the single a-C film and the multilayer films with $L_{a\text{-}C}/L_{WSx}$ ratio less than 1:9, while a violent fluctuation of the instantaneous friction coefficient of the multilayer films with $L_{a\text{-}C}/L_{WSx}$ ratio of 1:9 and 3:20 is found, especially at the later period of the test, suggesting that the two multilayer films are of inferior lubrication properties in humid air. In distilled water

(Fig.7c), the instantaneous friction coefficients of all the films are stable before an abrupt increase. However, the time at which the instantaneous friction coefficient increases abruptly is apparently shorter than those of the films in vacuum and in humid air.

Based on the data in Fig.7, the average (steady-state) friction coefficient is calculated in the sliding time range of 51-450s for the film in vacuum and in humid air and 51-350s for the film in distilled water and is illustrated in Fig.8a. As an exception, the sliding time range of 51-200s is used for the single a-C film in vacuum owing to its poor endurance life. As shown in Fig.8a, in vacuum, the single a-C film receives the highest average friction coefficient (~0.130) and the multilayer film with $L_{a\text{-}C}/L_{WS_x}$ ratio of 3:20 achieves the minimum value (~0.107), greater than the friction coefficient of the single WS_x film (~0.104), suggesting that the multilayered structure results in a higher friction coefficient. Graphite is well-known to have a high friction coefficient and a poor wear resistance in vacuum [46]. The fact that the single a-C film presents a friction coefficient comparable to graphite is easily understandable, since it has a similar structure to graphite. However, the decrease of the average friction coefficient of the multilayer film with an increasing $L_{a\text{-}C}/L_{WS_x}$ ratio from 1:39 to 3:20 is hardly to be understood. A possible explanation is that the lubrication property of the WS_x sublayer becomes better due to an increasing S/W ratio and decreasing oxygen content in the WS_x sublayer as increasing the $L_{a\text{-}C}/L_{WS_x}$ ratio. In humid air, the single WS_x film has an average friction coefficient of 0.237 and the single a-C film shows the lowest value (~0.118), while the friction coefficient of the

multilayer films gradually decrease from 0.261 to 0.165 with an increasing $L_{a\text{-}C}/L_{WSx}$ ratio. We can conclude that the increase of a-C content (*i.e.*, the decrease of WS_x content) in multilayer films can decrease the friction coefficient since the friction coefficient of the single a-C film is much lower than that of the single WS_x film in humid air. In distilled water, the dependence of the average friction coefficient with the $L_{a\text{-}C}/L_{WSx}$ ratio is very similar to the trend observed in humid air. By comparing the average friction coefficients of the multilayer films in the three test environments, one can see that the multilayer film has the lowest average friction coefficient in vacuum, and the highest average friction coefficient in humid air. A reasonable explanation for the latter is that the tribological property of the WS_x sublayer deteriorates more seriously in humid air than in distilled water and a limited anti-friction action of the a-C sublayer is presented in humid air. It should be noted that the average friction coefficients of the multilayer film with $L_{a\text{-}C}/L_{WSx}$ ratio of 1:39 and 1:19 are always higher than that of the single WS_x film in various test environments. The appearance of this phenomenon is likely caused by a relatively high content of oxygen in these films (see Table 1).

With respect to the wear resistance of the film in vacuum (Fig.8b), the wear rate of the single a-C film is close to that of the single WS_x film, while the wear rate of the multilayer films is about 8% ~ 10% of the single WS_x film and achieves the minima value ($5.7\times10^{-15}m^3\ N^{-1}m^{-1}$) at the $L_{a\text{-}C}/L_{WSx}$ ratio of 1:9. The possible reason for the better wear resistance of the multilayer films is that the multilayer film is of higher hardness than the single WS_x film (see Fig.5a), according to the Archard equation [47].

In humid air, the single a-C film has the best wear resistance and the wear rate of the multilayer films reaches the maximum value (4.5×10^{-14} m^3 $N^{-1}m^{-1}$) at the $L_{a\text{-}C}/L_{WSx}$ ratio of 3:20, which is only 1/3 ~ 1/4 of the value for the single WS_x film. The possible reason for the peaking of the wear rate of the multilayer films can be that the adhesion of the multilayer films decreases with the increase of $L_{a\text{-}C}/L_{WSx}$ ratio and a poor adhesion can easily lead to a delamination failure of the film. The single a-C film exhibits an excellent wear resistance in the atmosphere of water vapor and oxygen thanks to the dense structure and chemical inertia towards the environment. In distilled water, the wear rate of the multilayer films is obviously lower than that of the single WS_x film and slowly drops to the lowest value (1.2×10^{-13} m^3 $N^{-1}m^{-1}$) at the $L_{a\text{-}C}/L_{WSx}$ ratio of 1:4. The best wear resistance obtained with the sample ($L_{a\text{-}C}/L_{WSx}$ ratio = 1:4) is attributed to the highest content (or volume percentage) of a-C in the multilayer films, since the wear rate of the single a-C film (3.7×10^{-14} m^3 $N^{-1}m^{-1}$) is about 10 times lower than that of the single WS_x film (4.1×10^{-13} m^3 $N^{-1}m^{-1}$) in distilled water, demonstrating that the wear resistance of a-C film is much better than that of the single WS_x film in this condition. However, it can be seen that the wear rate is quite constant for different multilayer films. The possible reason is that the film's wear rate in distilled water is about 3 ~ 4 times higher than in humid air and the actual difference among the wear resistances of these films cannot be presented accurately due to a rather thin thickness of the films.

By comparing the wear rates of the film in different environments, one can see that the single WS_x film is of the best wear resistance in vacuum, the wear rate in

humid air or distilled water is 1.8 or 5.4 times higher than in vacuum. The single a-C film exhibits the best wear resistance in humid air and the wear rate in vacuum or in distilled water is 6.4 or 2.9 times higher than in humid air. As for the multilayer films, the wear resistance of the films in vacuum is much better than in humid air or in distilled water. Since the wear rates of different multilayer films under three test environments are much lower than those of single WS_x film and the friction coefficients are close to or even lower than that of single WS_x film, it can be concluded that the WS_x/a-C multilayer films are of better tribological properties and longer lifetime compared with single WS_x film.

4. Conclusions

WS_x/a-C multilayer films with different layer thickness ratios have been successfully prepared by magnetron sputtering method. The effects of $L_{a\text{-}C}/L_{WSx}$ ratio on the microstructure of as-prepared films are negligible while the effects on the mechanical and tribological properties are significant. The WS_x/a-C multilayer films are of the best wear resistance in vacuum and exhibit much better tribological properties than single WS_x film in various environments.

Acknowledgements

This research was supported by Zhejiang Provincial Natural Science Foundation of China under Grant No. LY15E010007.

Reference

[1] J.S. Zabinski, M.S. Donley, S.V. Prasad, N.T. Mcdevitt, Synthesis and characterization of tungsten disulphide films grown by pulsed-laser deposition, J. Mater. Sci. 29(1993) 4834–4839.

[2] T. Spalvins, Coatings for wear and lubrication, Thin Solid Films 53(1978) 285–300.

[3] S.V. Prasad, N.T. McDevitt, J.S. Zabinski, Tribology of tungsten disulfide films in humid environments: The role of a tailored metal-matrix composit substrate, Wear 230(1999) 24–34.

[4] S.R. Cohen, L. Rapoport, E.A. Ponomarev, H. Cohen, T. Tsirlina, R. Tenne, C. Levy-Clement, The tribological behavior of type II textured MX_2 (M=Mo, X=S, Se) films, Thin Solid Films 324(1998) 190–197.

[5] R. Gilmore, M.A. Baker, P.N. Gibson, W. Gissler, M. Stoiber, P. Losbichler, C. Mitterer, Low-friction TiN-MoS_2 coatings produced by dc magnetron co-deposition, Surf. Coat. Technol. 108(1998) 345–351.

[6] B. Deepthi, Harish C. Barshilia, K.S. Rajam, Manohar S. Konchady, Devdas M. Pai, Jagannathan Sankar, Alexander V. Kvit, Structure, morphology and chemical composition of sputter deposited nanostructured Cr-WS_2 solid lubricant coatings, Surf. Coat. Technol. 205(2010) 565–574.

[7] X.H. Zheng, J.P. Tu, D.M. Lai, S.M. Peng, B. Gu, S.B. Hu, Microstructure and tribological behavior of WS_2-Ag composite films deposited by RF magnetron sputtering, Thin Solid Films 516(2008) 5404–5408.

[8] Q. Wang, J.P. Tu, S.C. Zhang, D.M. Lai, S.M. Peng, B. Gu, Effect of Ag content on microstructure and tribological performance of WS_2-Ag composite films, Surf. Coat. Technol. 201(2006) 1666–1670.

[9] S. Xu, X. Gao, M. Hu, D. Wang, D. Jiang, J. Sun, F. Zhou, L. Weng, W. Liu, Microstructure evolution and enhanced tribological properties of Cu-doped WS_2 films, Tribol. Lett. 55(2014) 1–13.

[10] T.W. Scharf, A. Rajendran, R. Banerjee, F. Sequeda, Growth, structure and friction behavior of titanium doped tungsten disulphide (Ti-WS_2) nanocomposite thin films, Thin Solid Films 517(2009) 5666–5675.

[11] A. Nossa, A. Cavaleiro, Mechanical behaviour of W-S-N and W-S-C sputtered coatings deposited with a Ti interlayer, Surf. Coat. Technol. 163-164(2003) 552-560.

[12] A. Nossa, A. Cavaleiro. The influence of the addition of C and N on the wear behaviour of W-S-C/N coatings, Surf. Coat. Technol. 142-144(2001) 984-991.

[13] M. Evaristo, A. Nossa, A. Cavaleiro. W-S-C sputtered films: Influence of the carbon alloying method on the mechanical properties, Surf. Coat. Technol. 200(2005) 1076-1079.

[14] T. Polcar, M. Evaristo, A. Cavaleiro, Friction of self-lubricating W-S-C sputtered coatings sliding under increasing load, Plasma Processes Polym. 4(2007) s541–s546.

[15] J.V. Pimentel, T. Polcar, M. Evaristo, A. Cavaleiro, Examination of the tribolayer formation of a self-lubricant W-S-C sputtered coating, Tribol. Int. 47(2012)

188–193.

[16] J.H. Wu, D.A. Rigney, M.L. Falk, J.H. Sanders, A.A. Voevodin, J.S. Zabinski, Tribological behavior of WC/DLC/WS_2 nanocomposite coatings, Surf. Coat. Technol. 188(2004) 605–611.

[17] A.A. Voevodin, J.P. O'Neill, J.S. Zabinski, WC/DLC/WS_2 nanocomposite coatings for aerospace tribology, Tribol. Lett. 6(1999) 75–78.

[18] S. Watanable, J. Noshiro, S. Miyake, Tribological characteristics of WS_2/MoS_2 solid lubricating multilayer films, Surf. Coat. Technol. 183(2004) 347–351.

[19] S. Watanable, J. Noshiro, S. Miyake, Friction properties of WS_2/MoS_2 multilayer films under vacuum environment, Surf. Coat. Technol. 188-189(2004) 644–648.

[20] L.N. Zhu, C.B. Wang, H.D. Wang, B.S. Xu, D.M. Zhuang, J.J. Liu, G.L. Li, Microstructure and tribological properties of WS_2/MoS_2 multilayer films, Appl. Surf. Sci. 258 (2012) 1944–1948.

[21] D.C. Chen, B.L. Jiang, H.Y. Shi, Y.N. Long, Effect of ion cleaning pretreatment on interface microstructure, adhesive strength and tribological properties of GLC coatings on Al substrates, Vacuum 86(2012) 1576–1582.

[22] T. Polcar, M. Evaristo, A. Cavaleiro, The tribological behavior of W-S-C films in pin-on-disk testing at elevated temperature, Vacuum 81(2007) 1439–1442.

[23] J.R. Lince, P.D. Fleischauer, Crystallinity of rf-sputtered MoS_2 films, J. Mater. Res. 2(1987) 827–838.

[24] P.D. Fleischauer, Fundamental aspects of the electronic structure, materials properties and lubrication performance of sputtered MoS_2 films, Thin Solid

Films 154(1987) 309–322.

[25] H.A. Therese, J. Li, U. Kolb, W. Tremel, Facile large scale synthesis of WS_2 nanotubes from WO_3 nanorods prepared by a hydrothermal route, Solid State Sci. 7(2005) 67–72.

[26] C. Casiraghi, F. Piazza, A.C. Ferrari, D. Grambole, J. Robertson, Bonding in hydrogenated diamond-like carbon by Raman spectroscopy, Diam. Relat. Mater. 14(2005) 1098–1102.

[27] C. Casiraghi, A.C. Ferrari, J. Robertson, Raman spectroscopy of hydrogenated amorphous carbons, Phys. Rev. B 72(2005) 085401–085414.

[28] A.C. Ferrari, J. Robertson, Interpretation of Raman spectra of disordered and amorphous carbon, Phys. Rev. B 61(2000) 14095–14107.

[29] A.C. Ferrari, J. Robertson, Resonant Raman spectroscopy of disordered, amorphous, and diamond like carbon, Phys. Rev. B 64(2001) 075414–075426.

[30] S. Watanabe, J. Noshiro, S. Miyake, Friction properties of WS_2/MoS_2 multilayer films under vacuum environment, Surf. Coat. Technol. 188(2004) 644–648.

[31] R. Pandiyan, N. Delegan, A. Dirany, P. Drogui, M.A. El Khakani, Correlation of sp^2 carbon bonds content in magnetron-sputtered amorphous carbon films to their electrochemical H_2O_2 production for water decontamination applications, Carbon 94(2015) 988–995.

[32] E. Mounier, F. Bertin, M. Adamik, Y. Pauleau, P. B. Barna, Effect of the substrate temperature on the physical characteristics of amorphous carbon films deposited by d.c. magnetron sputtering, Diam. Relat. Mater. 5(1996) 1509–1515.

[33] F.P.J. M. Kerkhof, J.A. Moulijn, A. Heeres, The XPS spectra of the metathesis catalyst tungsten oxide on silica gel, J. Electron Spectrosc. Relat. Phenom. 14(1978) 453–466.

[34] V.R. Dhanak, A. Baraldi, G. Comelli, G. Paolucci, M. Kiskinova, R. Rosei, CO adsorption on unreconstructed and reconstructed Rh (110) surfaces: LEED and XPS studies, Surf. Sci. Lett. 295(1993) 287–294.

[35] C.D. Wagner, D.A. Zatko, R.H. Raymond, Use of the oxygen KLL Auger lines in identification of surface chemical states by electron spectroscopy for chemical analysis, Anal. Chem. 52(1980) 1445-1451.

[36] L. Salvati, L.E. Makovsky, J.M. Stencel, F.R. Brown, D.M. Hercules, Surface spectroscopic study of tungsten-alumina catalysts using x-ray photoelectron, ion scattering, and Raman spectroscopies, J. Phys. Chem. 85 (1981) 3700–3707.

[37] L. Benoist, D. Gonbeau, G. Pfister-Guillouzo, E. Schmidt, G. Meunier, A. Levasseur, XPS analysis of oxido-reduction mechanisms during lithium intercalation in amorphous molybdenum oxysulfide thin films, Solid State Ionics 76(1995) 81-89.

[38] D. Du, D. Liu, Z. Ye, X. Zhang, F. Li, Z. Zhou, L. Yu, Fretting wear and fretting fatigue behaviors of diamond-like carbon and graphite-like carbon films deposited on Ti-6Al-4V alloy, Appl. Surf. Sci. 313(2014) 462–469.

[39] M. Huang, X. Zhang, P. Ke, A. Wang, Graphite-like carbon films by high power impulse magnetron sputtering, Appl. Surf. Sci. 283(2013) 321–326.

[40] G. Zhang, P. Yan, P. Wang, Y. Chen, J. Zhang, The preparation and mechanical

properities of Al-containing a-C:H thin films, J. Phys. D: Appl. Phys. 40 (2007) 6748–6753.

[41] S. Xu, X. Gao, M. Hu, J. Sun, D. Wang, F. Zhou, L. Weng, W. Liu, Morphology evolution of Ag alloyed WS_2 films and the significantiy enhanced mechanical and tribological properties, Surf. Coat. Technol. 238(2014) 197–206.

[42] J.V. Pimentel, T. Polcar, M. Evaristo, A. Cavaleiro, Examination of the tribolayer formation of a self-lubricant W-S-C sputtered coating, Tribol. Int. 47(2012) 188–193.

[43] A. Katrib, F. Hemming, P. Wehrer, L. Hilaire, G. Maire, The multi-surface structure and catalytic properties of partially reduced WO_3, WO_2 and $WC+O_2$ or $W+O_2$ as characterized by XPS, J. Electron Spectrosc. Relat. Phenom. 76(1995) 195–200.

[44] R.F. Bunshah, Handbook of Hard Coatings-Deposition Technologies, Properties and Applications, Noyes Publication, New York, 2001.

[45] J.C. Sanchez-Lopez, D. Martinez-Martinez, C. Lopez-Cartes, A. Fernandez, Tribological behaviour of titanium carbide/amorphous carbon nanocomposite coatings: from macro to the micro-scale, Surf. Coat. Technol. 202(2008) 4011–4018.

[46] S. Miyake, Tribological properties of hard carbon films: extremely low friction mechanism of amorphous hydrogenated carbon films and amorphous hydrogenated SiC films in vacuum, Surf. Coat. Technol. 54(1992)563–569.

[47] J.F. Archard, Contact and rubbing of flat surfaces, J. Appl. Phys. 24(1953)

981–988.

Table captions

Table 1 The chemical components of the films

Table 1

$L_{a\text{-}C}$:L_{WSx}	S / at%	W / at%	C / at%	O / at%	S / W
WS_x	51.34	36.18	3.85	8.63	1.42
1:39	37.39	26.99	29.18	6.44	1.39
1:19	36.79	26.03	31.37	5.81	1.41
1:9	35.62	24.30	35.89	4.19	1.47
3:20	34.77	23.07	38.40	3.77	1.51
1:4	32.78	20.22	43.88	3.12	1.62
a-C	-	-	98.69	1.31	-

Figure captions

Fig.1. SEM morphologies of the films. (a) Surface (SE); (b) Cross-section (SE: WS_x, a-C; BSE: $L_{a\text{-}C}/L_{WSx}$=1:19, 1:4).

Fig.2. XRD patterns of the films.

Fig.3. Raman spectrum of the a-C layer of the multilayer film ($L_{a\text{-}C}/L_{WSx}$=1:19).

Fig.4. O1s (a), S2p (b), C1s (c) and W4f (d) photoelectron spectra and their fitting results of the multilayer film ($L_{a\text{-}C}/L_{WSx}$=1:19).

Fig.5. Hardness (a) and adhesive strength (b) of the films.

Fig.6. SEM morphologies of wear tracks of the films: Single WS_x (a-c), WS_x/a-C (d-i) single a-C (j-l).

Fig.7. The instantaneous friction coefficients of the films as a function of the sliding time.

Fig.8. Average friction coefficient (a) and wear rate (b) of the films in different environments.

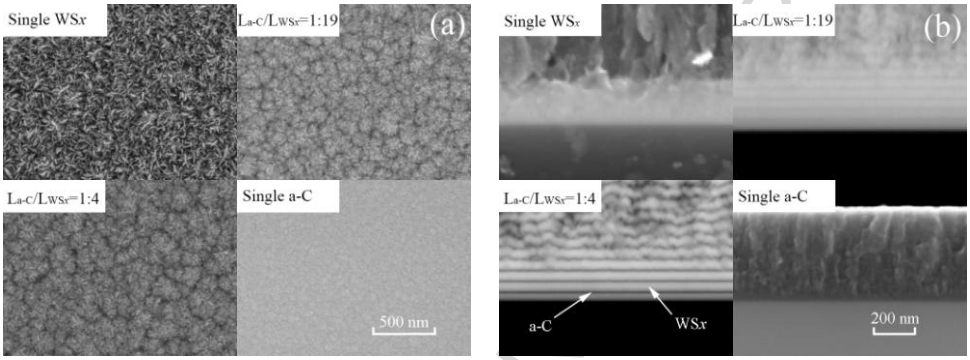

Fig.1

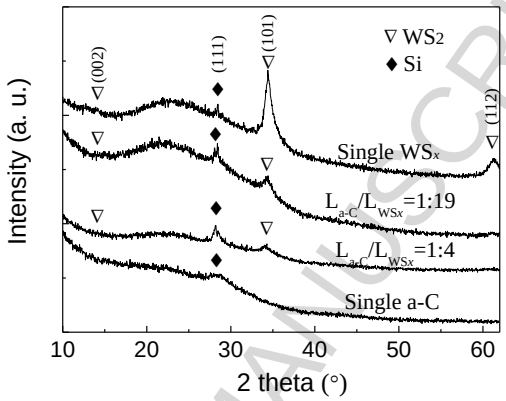

Fig.2

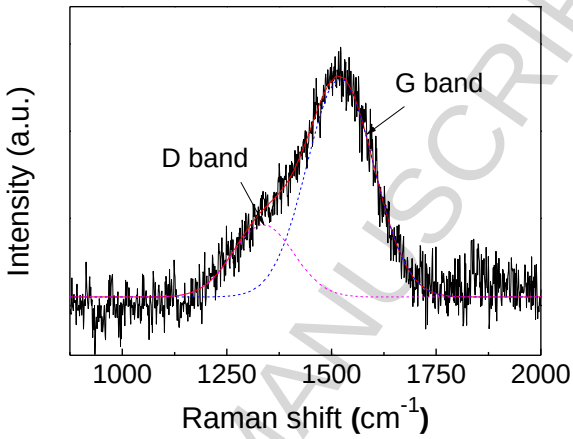

Fig.3

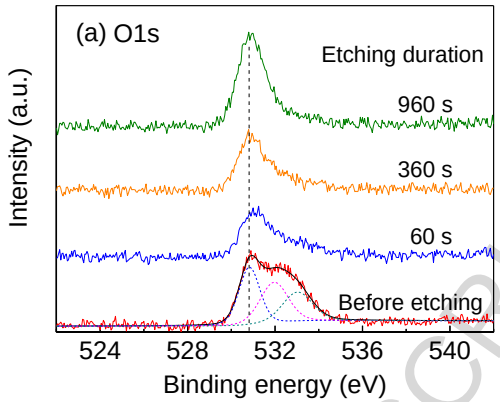

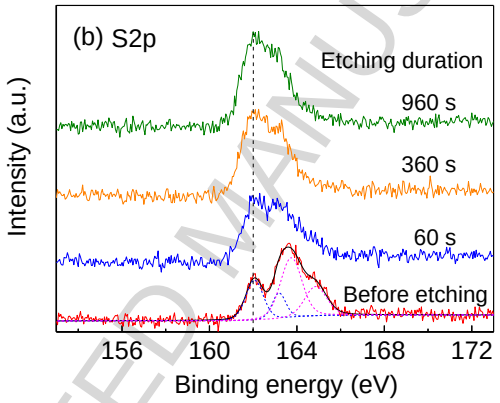

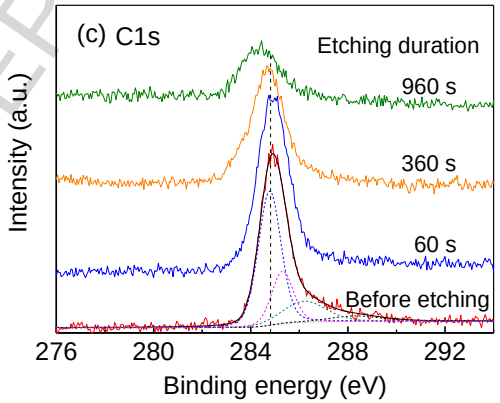

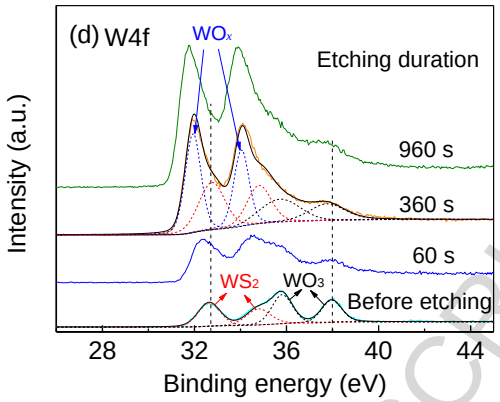

Fig.4

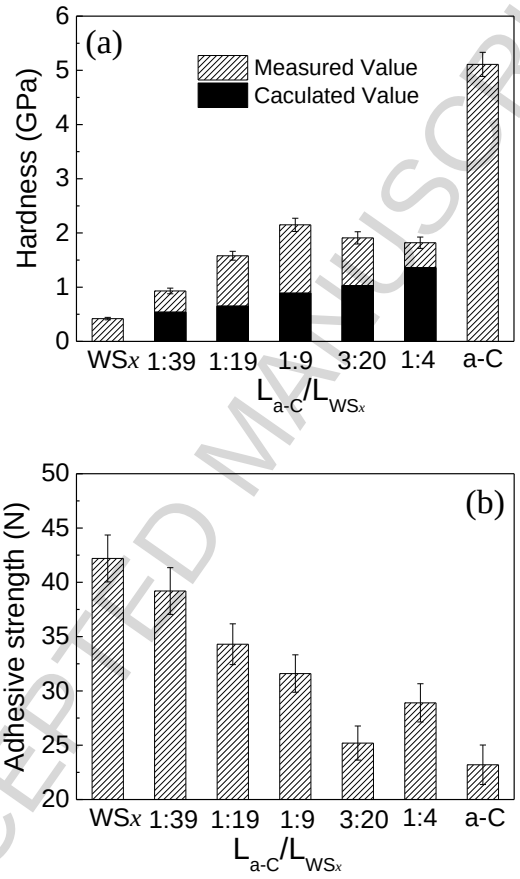

Fig.5

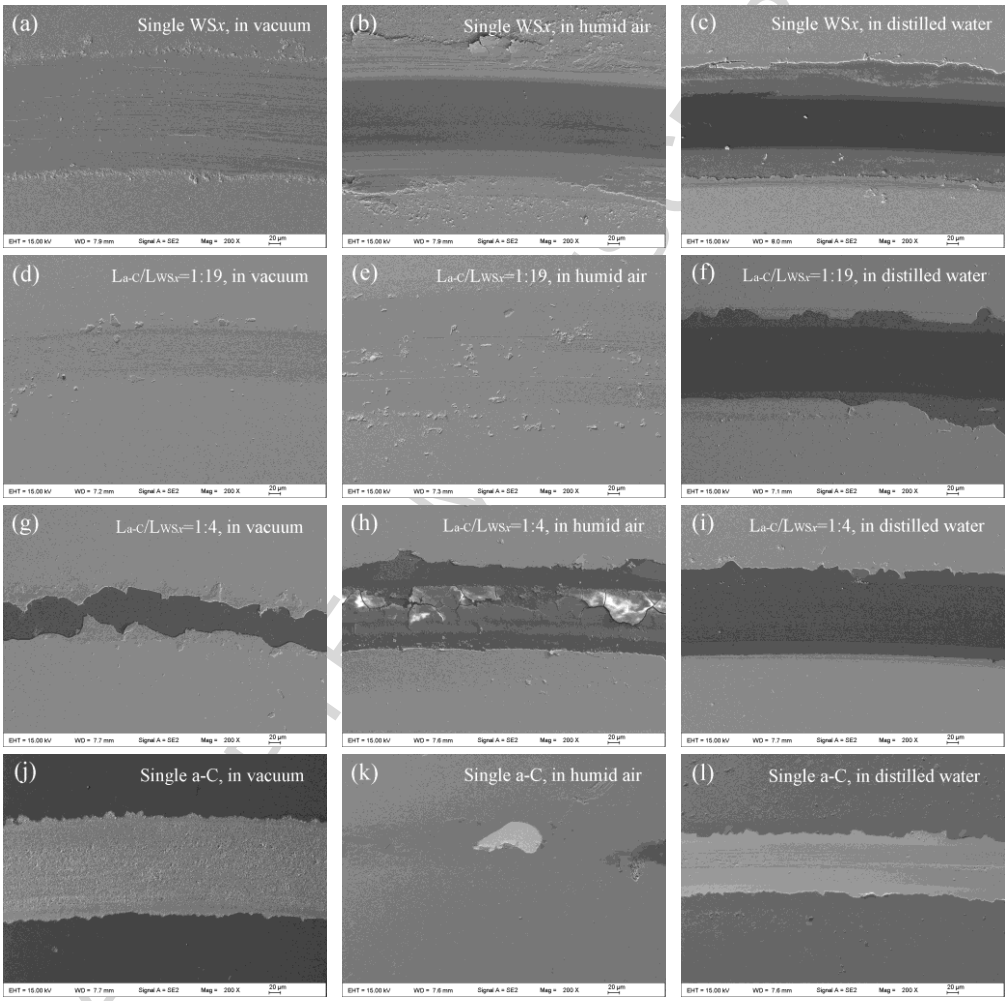

Fig.6

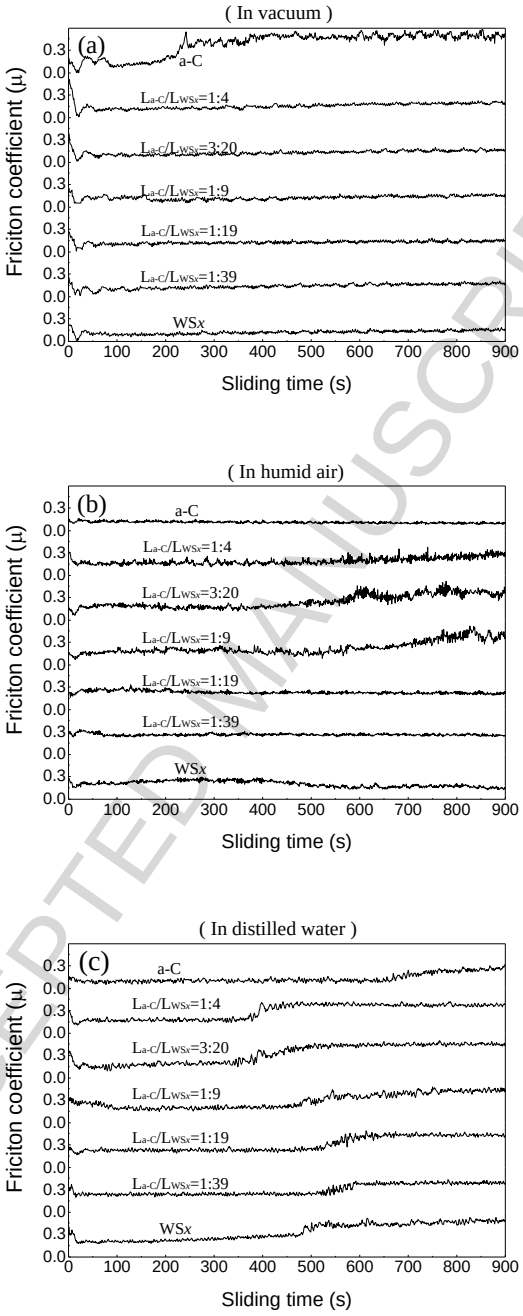

Fig.7

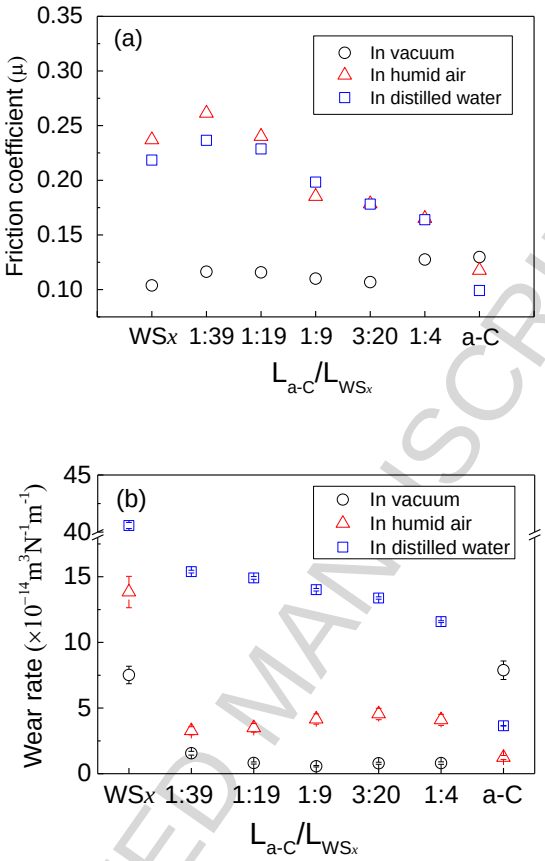

Fig.8

Highlights

- The nano-multilayered structure results in an increased harness but a decreased adhesion of the films.
- An increasing layer thickness ratio of a-C to WS_x raises the sulphur content of the WS_x sublayer.
- The effects of layer thickness ratio of a-C to WS_x on microstructure of the films are negligible.
- The WS_x/a-C multilayer films exhibit the best wear resistance in vacuum compared with in humid air and in distilled water.
- The tribological properties of the WS_x/a-C multilayer films are much better than single WS_x film in various test environments.